



Retrieving Stratospheric Ozone Profiles from OMPS Limb

2 Profiler Measurements

- 3 Fang Zhu¹, Xiaoping Liu¹, Suwen Li¹, Fuqi Si²
- 4 ¹Anhui Province Key Laboratory of Pollutant Sensitive Materials and Environmental Remediation, Anhui Province Key
- 5 Laboratory of Intelligent Computing and Applications, School of Physics and Electrical Information, Huaibei Normal
- 6 University, Huaibei, 235000, Anhui, China
- 7 Centre of Environmental Optics, Anhui Institute of Optics and Fine Mechanics, Hefei Institutes of Physical Science,
- 8 Chinese Academy of Sciences, Hefei, Anhui 230031, China
- 10 Correspondence to: Fang Zhu (zhufang160@163.com)
- 11 Abstract. This study describes a retrieval algorithm combining wavelength pairing and the multiplicative algebraic
- 12 reconstruction technique (MART) to process Ozone Mapping and Profiler Suite (OMPS) limb observations for vertical
- 13 ozone profiles. The retrieval algorithm employs scattered solar radiance measurements from the OMPS limb profiler,
- 14 focusing on the visible spectral range, normalizes this radiance to that at the upper tangent height, and retrieves ozone
- 15 concentrations between 12-40 km (~1 km vertical resolution). Additionally, it enables the identification of
- 16 cloud-contaminated measurements at specific altitudes within the instrument's field of view. The retrieval error in the
- 17 upper troposphere attributed to the prior profile is estimated to be 10-25%, while a 30% uncertainty in the aerosol
- 18 extinction coefficient causes ~5% error at 15-25 km. OMPS data spanning the entire year of 2021 are processed, and the
- 19 results are evaluated through comparisons with multiple independent datasets, including NASA official products, passive
- 20 satellite observations, and in-situ measurements from balloon-borne ozonesondes. At 17-36 km, deviations from
- 21 OMPS/LP v2.6 data are ≤5%; at 18–35 km, consistency with Microwave Limb Sounder (MLS) v5.0 data ranges from 5–
- 22 10%; at 20–35 km, most deviations from OSIRIS v7.3 data are ≤5% (except near 23 km). Comparisons with ozonesonde
- measurements reveal that differences in the 13-30 km range over northern mid-to-high latitudes are mostly <10% (with
- 24 10–15% differences at 22–25 km in polar regions). Over southern mid-latitudes, the consistency within the same altitude
- 25 range is 2-10%. Notably, deviations between the retrieved profiles and comparison products increase significantly in
- 26 low-altitude tropical regions.

1 Introduction

27

28

29

30

31

32

33

34

35

36

37

Stratospheric ozone forms a natural barrier protecting life on Earth by absorbing solar ultraviolet (UV) radiation (Arosio et al., 2018). Additionally, as a key greenhouse gas, it participates in the absorption and emission of infrared radiation in the stratosphere, playing a crucial role in regulating Earth's energy balance and stabilizing the climate system (Li et al., 2023). Dynamic changes in stratospheric ozone concentrations not only directly reflect the emission fluxes and chemical reaction processes of various atmospheric substances, but also serve as an important indicator for assessing the impact of human activities on the atmospheric environment (Young et al., 2021; Chipperfield and Bekki, 2024). Since the identification of the Antarctic ozone hole in the 1980s, research on the evolution patterns and driving mechanisms of stratospheric ozone concentration has remained a core topic in atmospheric science, attracting global research efforts to continuously explore its variation mechanisms and ecological effects.

High-precision retrieval of stratospheric ozone vertical profiles is a core requirement for advancing stratospheric



39

40

41

42

43

44

45

46

47

48

49

50

51

52

53

54

55

56

57

58

59

60

61

62

63

64

65

66

67

68

69

70

71

72

73

74

75

76



ozone research and establishing long-term essential climate variable datasets (Jia et al., 2015). To this end, multi-platform monitoring technologies—including ground-based, balloon-borne, airborne, and satellite-based instruments—have been widely applied over recent decades. Among these, satellite observations are categorized by detection modes into nadir, occultation, and limb observations. Nadir-viewing instruments, which detect downward, offer excellent horizontal coverage, with typical examples including the Ozone Monitoring Suite-Nadir (OMS-N) aboard Fengyun-3F (NSMC,2025), the Ozone Monitoring Instrument (OMI) aboard Aura(Veefkind et al., 2006), and the Environmental Monitoring Instrument (EMI) onboard the hyperspectral observation satellite GeoFen-5 (Qian et al., 2024). Occultation instruments, which directly view the solar disk, are represented by the Stratospheric Aerosol and Gas Experiment (SAGE III) (Cisewski et al., 2014), Atmospheric Chemistry Experiment (ACE) (Bernath et al., 2005), and Global Ozone Monitoring by Occultation of Stars (GOMOS) (Bertaux et al., 2010), featuring high vertical resolution and strong signal strengths. Limb scattering/emission observations combine the advantages of the aforementioned two modes, boasting high sensitivity, favorable vertical resolution, and high spatial sampling rates, such as the Microwave Limb Sounder (MLS) (Waters et al., 2006), SCanning Imaging Absorption spectroMeter for Atmospheric CartograpHY (SCIAMACHY) (Burrows et al., 1995), and Optical Spectrograph and InfraRed Imager System (OSIRIS) (Llewellyn et al., 2004). The Ozone Mapping and Profiler Suite (OMPS), a passive imaging spectrometer employed in this study, is onboard the Suomi-National Polar-orbiting Partnership (SNPP) satellite (Jaross et al., 2014). Its limb profiler (OMPS/LP) enables accurate retrieval of stratospheric ozone vertical profiles via limb observation mode. Since 2012, the NASA team has successively developed and released four versions of the ozone LP retrieval algorithm for OMPS limb observation data (the first version was released with operations (Rault et al,2013), the second version in 2014 (Xu et al.,2014), version 2.5 in 2017 (DeLand et al., 2017), and version 2.6 in 2023(Kramarova, 2023)). The University of Bremen has also applied its self-developed retrieval algorithm to OMPS/LP measurements (Arosio et al., 2018). In addition, another approach to processing OMPS/LP data employs a 2-D geometry retrieval method, as demonstrated in the work conducted at the University of Saskatchewan (Flynn et al., 2014).

This study focuses on ozone profile retrieval from OMPS/LP observation data, employing a retrieval algorithm based on wavelength pairing and the multiplicative algebraic reconstruction technique (MART). The algorithm is derived from the OSIRIS ozone profile retrieval scheme developed by the University of Saskatchewan. However, given the significant differences between OMPS/LP and OSIRIS in measurement technologies—including spectral resolution, spectral channels, wavelength range, atmospheric sampling, and radiance acquisition—this study has performed targeted optimizations and innovations on the algorithm, with entirely new developments in radiative transfer model construction, selection of retrieval spectra, and application of atmospheric parameter databases.

The research aims to verify the effectiveness of the wavelength pairing and MART algorithm in retrieving OMPS/LP ozone profiles, laying a theoretical and technical foundation for integrating OMPS/LP and OSIRIS data to construct long-term continuous datasets. The structure of this paper is as follows: Section 2 details the characteristics of the OMPS instrument, discussing its observational geometric principles and key issues in L1 data calibration. Section 3 systematically elaborates on the retrieval algorithm, including its core framework, application strategy of cloud filters, and parameter setting methods for the radiative transfer model. Section 4 conducts multi-dimensional validation and statistical analysis of the retrievals in this study, combined with NASA ozone profile products, MLS, OSIRIS, and ozonesonde datasets. Finally, the main results, key findings are summarized, and potential directions for future algorithm improvement are outlined in the conclusions.





77 2 OMPS/LP Ozone Retrieval

2.1 OMPS/LP instrument

The OMPS instrument was successfully launched aboard the SNPP satellite on October 28, 2011(Zhu et al., 2025). The satellite operates in a sun-synchronous polar orbit at an average altitude of 833 km with a 13:30 local time ascending node, commencing routine scientific observations in early 2012 (Kramarova et al., 2022). The OMPS suite integrates three distinct sensors: the Nadir Mapper (NM), Nadir Profiler (NP), and Limb Profiler (LP) (Arosio et al., 2018). Among them, OMPS/LP is centrally aimed at retrieving the vertical distribution of ozone in the Earth's middle atmosphere with high precision, employing a limb observation mode to sound the atmosphere by scanning the edge of the Earth's atmosphere. During a limb observation, the sensor's line-of-sight intersects the Earth's surface at a specific location, which is termed the tangent point (TP). The vertical distance from this point to the Earth's geoid is referred to as the tangent height (TH). The fundamental geometry of this observation mode is depicted in Fig. 1a.

The spectral coverage of OMPS/LP ranges from 290 nm to 1000 nm, with spectral resolution varying by wavelength—reaching 1.5 nm at the short-wavelength end and 40 nm at the longer-wavelength end (Kramarova et al., 2014). Equipped with a charge-coupled device (CCD), the instrument can simultaneously observe scattered solar radiation across the full spectral range at altitudes from 0 to 100 km. Each detector pixel possesses an instantaneous vertical field of view of approximately 1.5 km. This configuration enables a high-precision vertical sampling resolution of 1 km at the tangent point. (Jaross et al., 2014). To expand cross-track coverage, OMPS/LP is configured with three observation slits horizontally spaced by 4.25 ° (approximately 250 km), whose observational geometry and field-of-view characteristics are illustrated in Fig. 1b. Each slit has a 1.85 ° vertical field of view (FOV), corresponding to a 110 km vertical observation range at the TP. This study focuses on measurement data from the central slit, which is aligned with the satellite's ground track. The SNPP satellite operates in 14 orbits daily, with OMPS/LP completing approximately 160–180 measurements per orbit (at a latitudinal sampling interval of ~1 °). LP can achieve global coverage every 3–4 days (Kramarova et al., 2024).

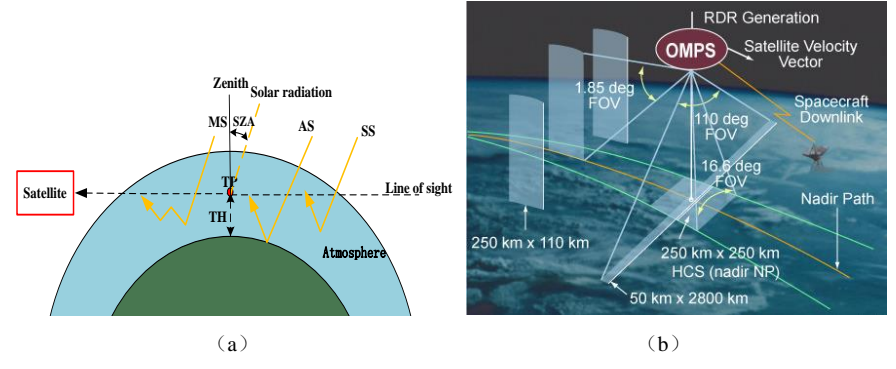


Figure 1. (a) Schematic of the satellite limb observation geometry, indicating the key parameters of tangent point (TP) and tangent height (TH) (SS: single scattering, AS: albedo scattering, MS: multiple scattering, SZA: solar zenith angle) (adapted from Arosio et al., 2018); (b) Schematic diagram of OMPS observation geometry and field-of-view characteristics (Kramarova et al., 2018).





2.2 OMPS LP L1 calibration

Radiometric errors and sensor pointing errors (primarily involving altitude registration errors) are the two main error sources affecting the accuracy of ozone profile retrieval via limb scattering techniques (Kramarova et al., 2024). In this section, we describe the instrument calibration in OMPS/LP L1G v2.6 processing.

Sensor pointing information is primarily acquired via the dual star trackers in the SNPP spacecraft's attitude determination system. However, misalignment between the attitude control frame and the fuselage frame, as well as thermally induced deformation of LP optical components, can lead to significant pointing offsets. To address this, multi-point corrections are implemented in L1G data processing following the method by Moy et al. (2017). The v2.6 version employs three types of corrections: static, intra-orbit, and time-dependent. The static correction for the central slit is 1.58 km. Intra-orbit corrections are based on the absolute radiometric residual method (ARRM) with linear adjustments along the south-north direction of the orbit; time-dependent corrections apply a uniform offset of +0.1 km.

Two-dimensional CCD detectors are susceptible to interference from internally scattered stray light, causing photons from intense light regions in the scene to scatter into weak signal areas. Jaross et al. (2014) proposed a stray light (SL) correction scheme based on pre-launch point spread function (PSF) measurements. The version 2.6 increases the intensity of the PSF tail in the UV and VIS/NIR bands by approximately 12%, correcting the bias in estimating stray light photons at high altitudes (Kramarova et al., 2024). In the VIS/NIR wavelengths, the central slit of the LP also incorporates a correction factor of 1.5 to account for in-band scattering, which may result from particle contamination on the primary telescope mirror. Additionally, although thermally induced changes in the optical pointing of the spectrometer can cause wavelength shifts at the center of the pixel band, this shift has a low correlation with altitude, and its impact on height-normalized measurements in ozone retrieval is negligible.

3 Retrieval method

3.1 Retrieval vector

The retrieval method for vertical ozone concentration distributions based on OMPS/LP measurements in this study draws on the technical framework developed by Zhu et al.(2021), who derived ozone number density profiles using SCIAMACHY limb scattering measurements in the Chappuis–Wulf band. It shares similar methodological principles with the approaches proposed by Roth et al. (2007) and Degenstein et al. (2009), all of which employ retrieval vectors positively correlated with ozone concentrations for calculations.

The first step in the retrieval process involves normalizing the limb radiance at selected wavelengths. This operation entails normalizing the limb radiance at each wavelength to a reference TH, which effectively eliminates interference from the solar Fraunhofer structure, weakens the impact of surface reflection, and simultaneously achieves instrument self-calibration (Jia et al., 2015).

136
$$I_{\text{nor}}(\lambda, H) = I(\lambda, H)/I(\lambda, H_{\text{ref}})$$
 (1)

where, H denotes the TH, and λ represents the wavelength. $I(\lambda, H_{\text{ref}})$ and $I_{\text{nor}}(\lambda, H)$ refer to the radiance at the reference TH and the normalized radiance, respectively. The reference TH is an upper altitude where ozone sensitivity is low; in this study, it is selected as 40.5 km (i.e., the reference TH above the maximum retrieval altitude). Although radiance normalization cannot completely eliminate the influence of surface reflection, it significantly reduces the requirements for modeling accuracy (Flittner et al., 2000). To mitigate the effect of aerosol scattering, the Chappuis





triplet vector (CTV) method proposed by Degenstein et al. (2009) is employed for wavelength pairing. In the Chappuis-Wulf band, the CTV is defined as the difference between the logarithmic average of normalized radiances at two weakly ozone-absorbing wavelengths and the logarithm of the normalized radiance at a wavelength near the ozone absorption peak, thereby enhancing the specificity of the retrieval signal. It is expressed as:

$$y_j = \ln \left(\frac{\sqrt{I_{\text{nor}}(\lambda_{\text{ref}_2}, j) \cdot I_{\text{nor}}(\lambda_{\text{ref}_2}, j)}}{I_{\text{nor}}(\lambda_p, j)} \right)$$
(2)

where, j denotes the index of the TH measured by the instrument, and y_j represents the retrieval vector after wavelength pairing at the j^{th} of TH. λ_{ref1} , λ_{ref2} , and λ_{p} correspond to the weakly ozone-absorbing reference wavelengths and the strongly absorbing peak wavelength, respectively. In this study, referencing the wavelength system by Kramarova et al. (2024) and the selection criteria by Zhu et al. (2021), λ_{ref1} is set to 512 nm, λ_{ref2} to 606.3 nm, and λ_{p} to 675.5 nm. The paired measurement vectors maintain high sensitivity to ozone concentration.

The CTVs and retrieved ozone profiles across different latitudes (Fig. 2) indicates that the values of CTV are highly correlated with the spatiotemporal distribution of ozone concentrations. The CTV peak in tropical regions occurs at a higher altitude than in mid-to-high latitudes, and the peak altitude decreases progressively with increasing latitude. The distribution range of CTV in polar regions expands synchronously with changes in ozone concentration. Additionally, CTV values near zero above 35 km exhibit insufficient sensitivity to ozone responses, resulting in poor performance in practical retrieval. Furthermore, CTV values above 40 km are negative and cannot be used for retrieval.

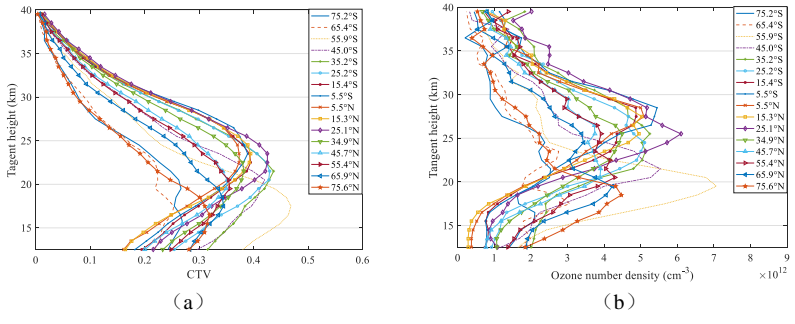


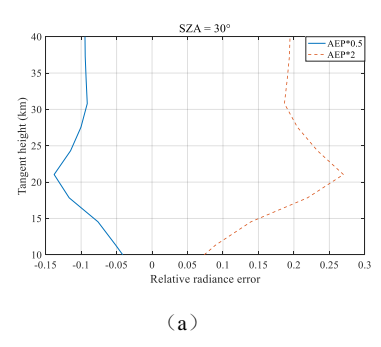
Figure 2. Samples of CTV and ozone profiles at different latitudes from orbit 51220 on September 15, 2021. (a) CTVs; (b) Retrieval ozone profiles.

Aerosols, as suspended particles capable of absorbing and scattering light, have sources including both natural and anthropogenic factors. Stratospheric aerosols mainly originate from SO₂, HCl released by volcanic eruptions, naturally generated OCS, and pollutants such as SO₂ from industrial emissions (Li et al., 2023). The presence of aerosols enhances the intensity of atmospheric scattered light, with the relative increment of red waves in the spectrum being higher than that of blue waves. Based on the SCIATRAN model (radiative TRANsfer model for SCIAMACHY), this study conducted simulation experiments on aerosol extinction coefficients to explore their impacts on radiance and CTV.

Fig. 3 shows the effects of aerosol extinction profiles with different multiples on radiance and CTV. When the aerosol profile varies within the range of 0.1-10 times the standard value, the radiance profile is positively correlated with the aerosol extinction coefficient, while CTV decreases as the extinction coefficient increases, with the impact mainly concentrated below 40 km. For instance, when the aerosol extinction profile doubles, the radiance value at 21 km increases by 27%, while CTV decreases by only 5%. It indicates that wavelength pairing can weaken the aerosol scattering effect but cannot completely eliminate it. In addition, the study found that both radiance errors and CTV errors increase with an increase in SZA.







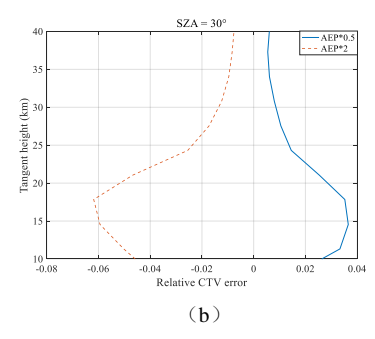


Figure 3. Variations in radiance and CTV with aerosol extinction coefficients of different multiples. (a) Relative radiance error; (b) Relative CTV error.

3.2 Multiplicative algebraic relaxation technology

Given the nonlinear nature of the retrieval problem, this study employs an iterative method for solution and selects the multiplicative algebraic reconstruction technique (MART) to perform ozone profile retrieval. As an improved algorithm of nonlinear relaxation techniques, MART has a main advantage in that it can utilize multiple sets of measurement vectors to realize the retrieval of atmospheric state parameters at any altitude (Roth et al., 2007). During the iteration process, the update of atmospheric states at each altitude depends on a multiplicative factor, which is obtained by weighted averaging the ratios of all valid observation vectors to simulation vectors. The general formula of the MART algorithm is as follows:

187
$$x_i^{(n+1)} = x_i^{(n)} \sum_j \left(\frac{y_j^{\text{obs}}}{y_j^{\text{mod}}} W_{ji} \right)$$
 (3)

where, $x_i^{(n)}$ denotes the ozone number density at atmospheric height i during the n^{th} iteration; y_j^{obs} and y_j^{mod} represent the observation vector and simulation vector processed via Equations (1) and (2), respectively, where \mathbf{y}^{mod} is generated by the radiative transfer model based on the ozone profile $\mathbf{x}^{(n)}$ obtained from the n^{th} iteration; W_{ji} is the line-of-sight weight factor, indicating the influence weight of the j^{th} TH or line of sight on atmospheric height i. At each altitude, $\sum_j W_{ji} = 1$. The value of W_{ji} in this study follows the setting in Zhu et al., (2021).

3.3 Cloud filter

A critical step in the OMPS/LP ozone profile retrieval is to define the lower boundary by determining cloud top height. This is accomplished using a cloud detection method, modified from Chen et al. (2016), which leverages the spectral contrast in radiance between red and near-infrared bands. The method quantifies this contrast by computing the change in the vertical radiance gradient between two selected wavelengths. The underlying premise of the gradient-based cloud detection algorithm is that clouds generate a significantly larger radiance gradient compared to aerosols. This gradient is quantitatively defined as the rate of change of radiance with respect to TH:

$$G(\lambda, H) = \partial \ln I(\lambda, H) / \partial H \tag{4}$$

As shown in Fig. 4a, the variation characteristics of radiance gradient with wavelength in the 500-900 nm provide a basis for determining cloud top height. In cloud-free conditions, the radiance intensity varies slightly with wavelength; whereas in the presence of clouds, the wavelength dependence of radiance is significantly stronger than that of aerosols. Based on this, in this study, the cloud top height is determined by calculating the spectral gradient difference, with the formula as follows:





 $\ln \mathbf{R}(H) = [\mathbf{G}(\lambda_{S}, H) - \mathbf{G}(\lambda_{I}, H)] \tag{5}$

where, λ_s and λ_l denote the short wavelength and long wavelength, respectively. In this study, λ_s is set to 674 nm, and λ_l is set to 868 nm. The positive cloud detection threshold for LP data is 1.5, which is also applicable to the detection of polar mesospheric clouds (PMCs). Taking the SNPP satellite orbit 51220 on September 15, 2021 as an example (Fig.4b), the characteristics of lnR profiles differ significantly between two cloudy events and one cloud-free event: the maximum value of lnR in the cloud-free event is below 1.5, while that in the cloudy events is above this threshold, and the TH corresponding to the maximum lnR value is the cloud top height. During the ozone retrieval process, the multiplication factor of the ozone profile below the cloud top height remains unchanged.

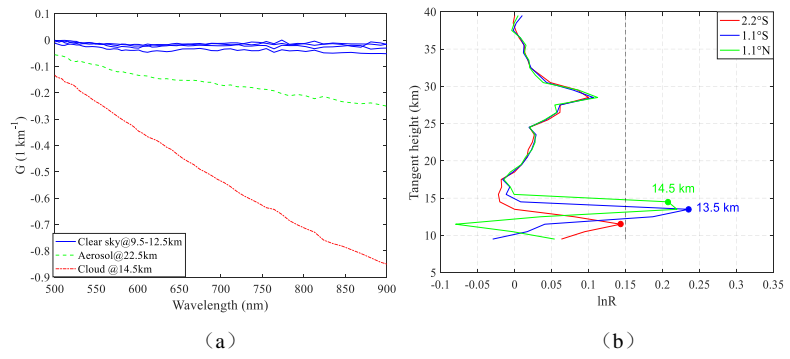


Figure 4. Radiance gradient $G(\lambda, H)$ and gradient difference $\ln R$ during orbit 51220 on September 15, 2021. (a) Radiance gradient $G(\lambda, H)$ spectrum at 3 N under different atmospheric conditions: clear sky (blue), cloud (red), and aerosol (green); (b) Radiance gradient difference $\ln R$ derived from OMPS/LP measurements for three equatorial events, showing the cloud detection results. The black dashed line represents the threshold employed for cloud identification.

3.4 Implementation details

In this study, the SCIATRAN v2.2 toolbox (Rozanov et al., 2017) is employed as the forward modeling to calculate the simulated radiances required for ozone concentration retrieval. The observed and simulated radiances are processed through normalization and wavelength pairing to form retrieval vectors, which serve as inputs to the MART algorithm to drive the iterative update of ozone profiles.

The radiative transfer solution in the forward model is based on the discrete ordinate method applied to a spherical atmosphere. The solution incorporates the effects of multiple scattering and refraction while explicitly omitting polarization. Radiance calculations in the model are focused solely on ozone, an absorbing gas, with the ozone absorption cross-sections referenced from the research results of Bogumil et al. (2000). The pressure and temperature profiles used in this study were obtained from the Global Modeling and Assimilation Office (GMAO) interpolated dataset. These meteorological data are incorporated in the OMPS/LP L1G dataset provided by NASA (NASA, 2025a). In addition, the model sets the stratospheric background aerosol type as LOWTRAN (Kneizys, 1986), the boundary layer humidity as 80%, and the boundary layer aerosol type as marine. The vertical resolution of the ozone profile retrieval is fundamentally constrained by the native resolution of the input data. Given that the OMPS/LP L1G data are provided on a fixed 1 km TH grid, the resulting profiles consequently exhibit a vertical resolution of 1 km. The prior profiles are from SCIATRAN's built-in database. These profiles are provided by McLinden climatology (C. McLinden, Meteorological Service of Canada, personal communication) and include monthly and latitude-dependent vertical distributions of volume mixing ratios for O₃, NO₂, BrO, and OClO, as well as pressure and temperature in the 0 to 100 km altitude range. The volume mixing ratio of ozone can be converted to ozone number density based on temperature and pressure.





239 4 Results

 This section presents the processing results derived from the full year of 2021 OMPS-LP data. We utilized the L1G v2.6 dataset (Jaross, 2023), which incorporates enhanced stray light correction and pointing accuracy as detailed in Section 2.2. The analysis is based exclusively on measurements from the instrument's central slit.

4.1 Error analysis

In the field of error research on limb-scattering ozone retrieval, there is a wealth of academic achievements. Zhu et al. (2022) used numerical perturbation technology to conduct formal error analysis on the retrieval method of the weighted multiplicative algebraic reconstruction technique, accurately quantifying ozone retrieval errors at different altitudes. Arosio et al. (2022) systematically evaluated random errors and systematic errors for stratospheric ozone profile retrieval based on DOAS and OE algorithms. These research results provide important references for the error analysis of MART retrieval algorithm, and the error estimation results of this study are consistent with those in Arosio et al. (2022) and Zhu et al. (2022).

To ensure data quality, radiance measurements contaminated by clouds were systematically excluded during retrieval. Furthermore, the scene reflectance was determined directly from OMPS/LP radiance measurements at 675 nm. The corrected THs in NASA L1G data are adopted. Therefore, the estimation of the total retrieval error of ozone profiles focuses on such factors as prior profiles, aerosols extinction profile, ozone absorption cross-sections, and measurement noise.

Understanding the impact of the initial ozone profile on retrieval results is crucial. In this study, the prior average kernel matrix \mathbf{A}_0 is used to quantify the sensitivity of retrieval to the prior, and its expression is as follows:

$$\mathbf{A}_0 = \frac{\partial \hat{\mathbf{x}}}{\partial \mathbf{x}_0} \tag{6}$$

where x_0 and \hat{x} represent the initial ozone profile and the retrieved ozone profile, respectively. To calculate the column vectors of A_0 , the ozone concentration at a single altitude was perturbed in x_0 by 5% and analyzes the corresponding changes in \hat{x} . A_0 is a dimensionless matrix, whose characteristics can intuitively reflect the impact of changes in the prior profile on the retrievals.

Fig. 5a illustrates the distribution of the prior average kernel matrix (\mathbf{A}_0) column vectors across the 12–40 km altitude range, with each curve plotted at a vertical resolution of 2 km. It indicates that at the lower boundary of retrieval, perturbations in the prior profile hardly induce significant responses in the retrieval results. Fig. 5b compares the relative retrieval errors under the conditions of prior profiles at low latitudes (5.5 %) and mid-latitudes (45 %), and it is found that the errors increase significantly at the lower boundary of retrieval, which is consistent with the analysis results of \mathbf{A}_0 . The prior errors of retrieved ozone profiles above 20 km have weak correlation with latitude, and the errors remain at 1-2% in the altitude range of 20-40 km; while at lower altitudes, especially in tropical and mid-latitude regions, the relative errors can reach 10-25% due to the rapid decrease of ozone concentration and the reduction of retrieval accuracy.



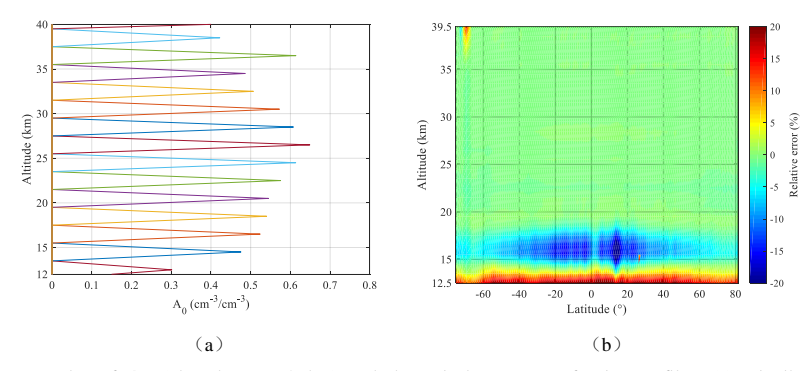


Figure 5. Examples of A_0 (plotted every 2 km) and theoretical accuracy of prior profiles. (a) Distribution of A_0 for measurements at 2.2 °S; (b) Variation of retrieval errors of prior profiles in mid-latitudes and low latitudes with latitude (orbit 51220 on September 15, 2021).

The uncertainty of stratospheric aerosol extinction coefficients requires consideration. Studies have demonstrated that retrieved aerosol extinction profiles exhibit an average upper error bound of approximately 30% in the lower stratosphere (Arosio et al., 2022). Fig. 6a illustrates the distribution characteristics of ozone retrieval errors with latitude and altitude under a 30% uncertainty in aerosol extinction coefficients. It is evident that retrieval errors induced by variations in aerosol extinction coefficients are predominantly distributed within the 15-25 km altitude range, with a magnitude of approximately 5%, and errors in the southern high latitudes are more pronounced. Within the 25-30 km range, the error is around 2%, while above 30 km, it is less than 1%. Below 15 km, errors vary with latitude, mostly falling within the range of ±2%.

Since ozone absorption cross-sections depend solely on temperature rather than pressure, it is necessary to investigate the impact of the temperature sensitivity of absorption cross-sections on ozone profile retrieval. Fig. 6b depicts the relative retrieval errors attributable to the difference between ozone absorption cross-sections at 243 K and 223 K, revealing that a 20 K temperature difference induces errors below 0.6% at all latitudes and altitudes. The most significant errors, though still minimal, are confined to altitudes below 18 km in tropical regions. A 1% perturbation was added to the retrieval vector to simulate measurement noise, and the resulting relative errors in ozone retrieval were calculated. As shown in Fig. 6c, retrieval errors caused by measurement noise do not exceed ±2% across all latitudes and altitudes; errors above 20 km are independent of latitude, while negative errors below 20 km are largest in tropical regions and decrease with increasing latitude.

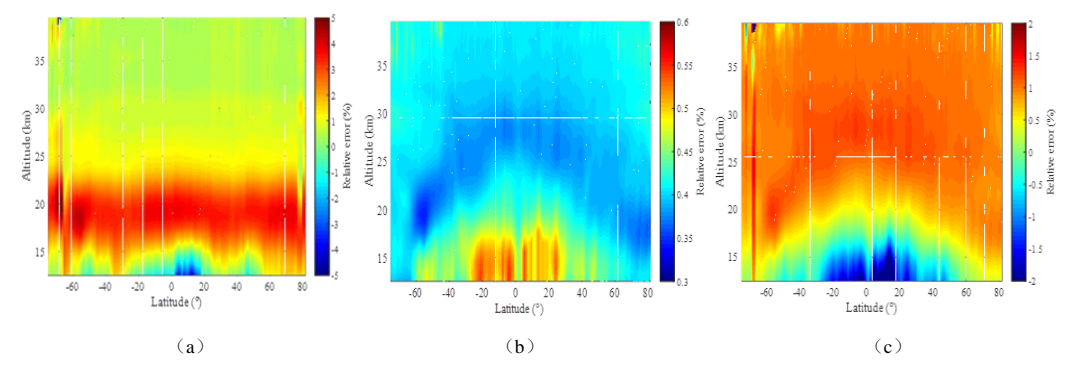


Figure 6. Distribution of relative errors in ozone retrieval with latitude and altitude. (a) Aerosol extinction coefficients; (b) Ozone absorption cross-sections; (c) Measurement noise.





4.2 Comparison with NASA OMPS-LP ozone product

The OMPS/LP v2.6 ozone profile retrieval algorithm developed by the NASA team is built on wavelength pairing and an optimal estimation with prior constraints (Kramarova and Deland, 2023). This algorithm operates on combined UV-Vis measurement data from 12.5 km (or cloud top) to 57.5 km, producing a single ozone profile from each retrieval. The measurement vectors are obtained via doublet and triplet methods, with specific parameters detailed in Table 1. During algorithm implementation, retrieved surface albedo, cloud top height, and corrected TH are integrated. In forward model, aerosol extinction coefficients retrieved from OMPS/LP measured data.

Table 1. Parameters used in the OMPS/LP v2.6 ozone algorithm, according to Kramarova and Deland, (2023).

Parameters	Values
Wavelength used in UV (nm)	295, 302, 306, 312, 317, 322, 353
Wavelength used in Vis (nm)	510, 606, 675
Normalization Altitude in UV (km)	60.5 km
Normalization Altitude in Vis (km)	40.5 km

Fig. 7 shows a comparison between the retrievals of this study and those of OMPS/LP v2.6, involving approximately 770,000 profiles. Among them, Fig. 7a presents an example of number density for the annual average profile, and Fig. 7b shows the relative differences of the annual data. In this study, the relative difference is calculated as follows:

309
$$E_{dif} = \frac{2 \cdot ([O_3]_{Ret} - [O_3]_{Ref})}{([O_3]_{Ret} + [O_3]_{Ref})} \times 100\%$$
 (7)

where $[0_3]_{Ret}$ denotes the ozone profile retrieved in this study, and $[0_3]_{Ref}$ represents the reference ozone profile product.

As presented in Fig. 7b, the ozone concentrations from our retrieval systematically exceed those of the OMPS/LP v2.6 product at altitudes below 19 km and above 35 km. The positive deviation increases with decreasing altitude, reaching a maximum of approximately 10-24% at the upper and lower boundaries of retrieval. The ozone concentration is slightly lower between 20 and 28 km, with a deviation within 3%. There is an inherent negative deviation of about -6% around ~33 km. Overall, the deviation between 17 and 36 km is controlled within 5%.

Fig. 8 shows the comparison between the retrievals of this study and OMPS/LP v2.6 in tropical regions and southern, northern mid-high latitudes. In the tropical region within the 18-36 km altitude range, the deviation is within 5%, showing good consistency. In the northern mid-latitude region, the difference between 12 and 32 km reaches 8%, and the difference above 32 km is as high as 8–13%, with similar deviations in the Arctic region. In the southern mid-high latitudes, most of the deviations above 18 km are less than 3%, but there is a positive deviation of up to 19% near 15 km. In the Antarctic region, this positive deviation extends to around 18 km, approximately 10%.

The two profiles differ significantly in the upper troposphere and lower stratosphere (UTLS) region, especially in the tropical region, mainly due to the extremely low ozone concentration at this altitude in low latitudes. The large positive deviation at the upper boundary of retrieval may be caused by the decreased ability of the visible spectrum to retrieve ozone at high altitudes, while the NASA product uses combined ultraviolet and visible spectrum information for retrieval at this altitude. Although there are differences between the retrievals of this study and the OMPS/LP v2.6 product in terms of ozone absorption cross-sections, prior profiles, aerosol settings, retrieval algorithms, and spectra, the overall consistency is high.





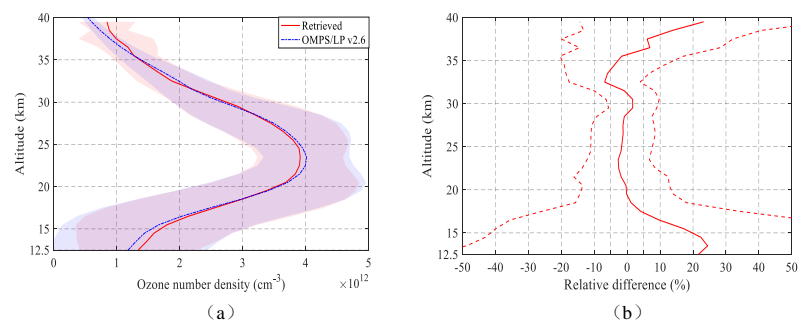


Figure 7. (a) Annual mean ozone number density profiles from this study and the OMPS/LP v2.6 product, with shaded areas indicating the standard deviation. (b) The corresponding annual mean relative differences, with the standard deviation shown as a dashed line.

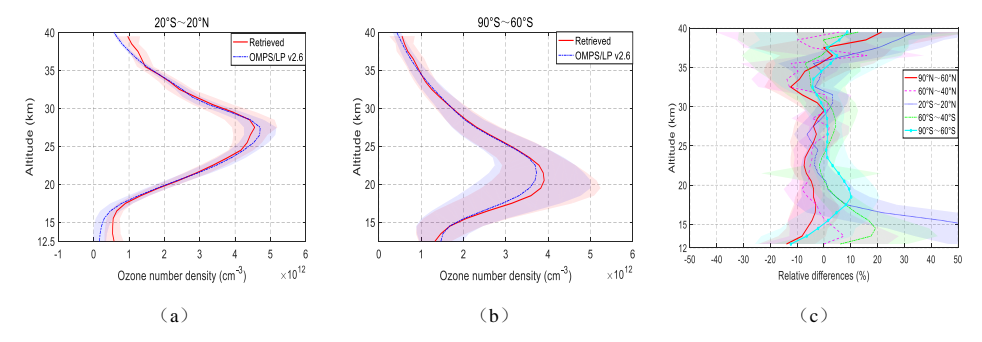


Figure 8. (a, b) Annual mean ozone number density profiles from this study and OMPS/LP v2.6 for the tropics and Antarctic, respectively. (c) Zonal mean relative differences across five latitudinal bands (60 °-90 N, 40 °-60 N, 20 S-20 N, 60 °-40 S, 90 °-60 S); standard deviations are shown as shaded areas.

4.3 Comparison with MLS

The Earth Observing System-Microwave Limb Sounder (EOS-MLS) aboard the Aura satellite was successfully launched on July 15, 2004 (Waters et al., 2006). The satellite operates along 14 orbits daily, achieving global coverage between 82 % and 82 %. The MLS obtained vertical ozone profiles from the upper troposphere to the middle atmosphere using the 240 GHz frequency band by detecting naturally emitted microwave thermal radiation from the Earth's atmospheric limb measurements. Detailed descriptions can be found by Waters et al. (2006).

For validation purposes, this study employs the latest MLS L2 version 5.0 data product (Schwartz et al., 2020), with data filtering applied in accordance with the protocols recommended by Livesey et al. (2022). To ensure collocation quality from the substantial dataset, stringent criteria were enforced: we retained only those data pairs where the geographical separation between the OMPS/LP and MLS footprints was within 1° in both latitude and longitude, and the observation time difference was less than 6 hours. In cases where multiple MLS profiles corresponded to a single OMPS/LP measurement, their average was computed and used. For consistent comparison with NASA products and ozonesonde data, the MLS volume mixing ratio (VMR) and pressure were first transformed to number density and altitude, utilizing the MLS geopotential height. These converted profiles were subsequently interpolated onto the regular altitude grid of the OMPS retrievals using a spline method.

Fig. 9 presents the average profiles and relative differences between the retrieval results of this study and MLS v5.0,





involving approximately 93,000 profiles. The results show that compared with MLS v5.0, the ozone concentration retrieved in this study has a relatively large positive deviation of 5–20% below 18 km; the positive deviation above 32 km increases with the increase in altitude; within the 18–35 km height range, the deviation between the two is controlled within 5%.

Fig. 10 shows the average profiles in the tropics and southern high latitudes, as well as the relative differences in five latitude zones, with shaded areas indicating the standard deviations. In terms of data sample size, there are approximately 18,000 profiles in the tropical region, about 20,000 in the northern high latitudes, and around 15,000 in the southern high latitudes. The analysis results reveal that within the 12–35 km height range, the zonal average relative differences in each latitude zone are basically controlled within 10%. Among them, the northern mid-high latitudes exhibit a stable negative deviation of 5–10% at 20–35 km; the southern mid-latitudes have a constant positive deviation of 1–5% at 18–36 km, which further expands to 3–10% in the polar regions. The tropical region shows obvious stratification characteristics: the retrieved ozone number density at 19–27 km is 5–10% lower than that of MLS, while it is 3–10% higher in the 28–36 km range. It is worth noting that below 19 km, the consistency between the retrieval results of this study and MLS data decreases significantly, with the relative difference in the tropical region even exceeding 30%, although the absolute difference is relatively small (see Fig. 10a).

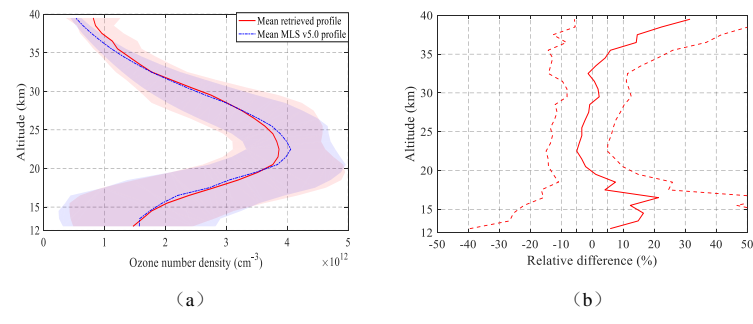


Figure 9. (a) Annual mean ozone number density profiles from this study and MLS v5.0, accompanied by standard deviations (shaded areas). (b) The corresponding annual mean relative differences, accompanied by standard deviations (dashed lines).

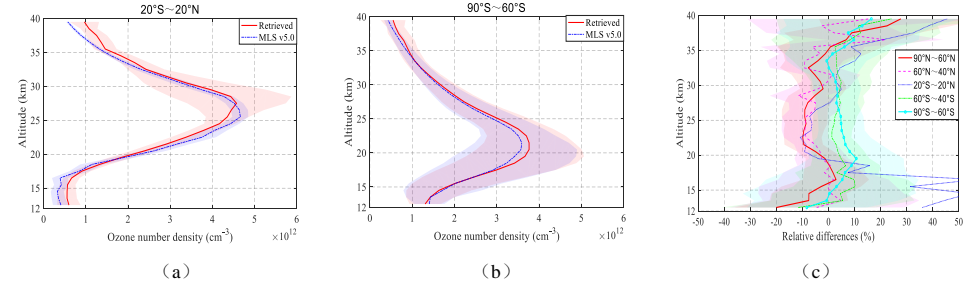


Figure 10. (a, b) Annual mean ozone number density profiles (this study vs. MLS v5.0) for the tropics and Antarctic, respectively. (c) Zonal mean relative differences for five latitudinal bands ($60^{\circ}-90^{\circ}N$, $40^{\circ}-60^{\circ}N$, $20^{\circ}-20^{\circ}N$, $60^{\circ}-40^{\circ}S$, $90^{\circ}-60^{\circ}S$); standard deviations as shaded areas.

Fig. 11 presents the variation of relative differences between retrieval profiles within 1 °latitude bins and MLS zonal averages with altitude, covering three time periods. The full-year 2021 data shown in Fig. 11a indicate that within the 20-35 km altitude range, differences across all latitudes are basically controlled within ±10%. Analyzing the difference characteristics from low to high altitudes: oscillating differences exceeding 30% appear in the tropical UTLS region, which may be caused by factors such as high dynamic changes in ozone concentration, insufficient detection sensitivity





in the lowest retrieval altitude segment, and cloud filtering effects; in addition, the low ozone concentration in this region also affects the accuracy of retrieval profiles. In the tropical region, there is a decreasing trend in retrieved ozone values at 20-23 km altitude, which is particularly significant in winter (see Fig. 11c); while higher values are observed in the Antarctic region, which may be related to albedo retrieval deviations at polar latitudes in winter. Above 35 km, retrievals in the tropical region are larger, and this interval corresponds to the overlapping area of ultraviolet and visible spectral windows, where the merging of data from the two may cause inconsistent results.

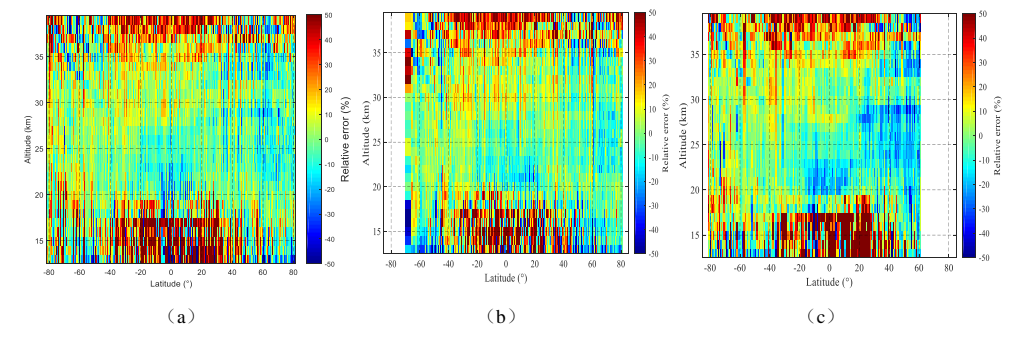


Figure 11. Relative differences in ozone number density, averaged over 1 °latitude bins and plotted as a function of altitude, for (a) the entire year of 2021, (b) the boreal summer months (June-August), and (c) December.

In summary, the comparative analysis of this study shows that the effectiveness of OMPS retrieval varies across different regions and altitudes: the effectiveness in tropical regions is concentrated in the 20-35 km altitude range; in mid-latitude regions, good consistency is also observed below 15 km. Nevertheless, in some atmospheric regions and under different seasonal conditions, the relative deviation may still exceed 10% compared with MLS data.

4.4 Comparison with OSIRIS

In February 2001, the OSIRIS instrument was launched aboard the Odin satellite into a nearly circular sun-synchronous orbit (Llewellyn et al., 2004). The orbit has an altitude of approximately 600 km, an orbital period of 96 minutes, an inclination of 97.8°, and covers an observational latitude range from 82 °S to 82 °N. The satellite's ascending node crosses the equator at approximately 18:00 local time. Detailed descriptions of the instrument can be found by Llewellyn et al., (2004). Degenstein et al. (2009) used the MART to retrieve ozone profiles in the altitude range from 10 km or cloud top to 60 km, with the retrieval algorithm integrating radiation information from the UV and VIS bands. In this study, the version of OSIRIS L2 v7.3 data (University of Saskatchewan, 2025) is used for verification.

Owing to the sparsity of coincident OSIRIS measurements, a relaxed collocation criterion was adopted. Data pairs were considered matched if the geographical distance between the instrument footprints was within 2° in latitude and 5° in longitude, and the time difference was within 24 hours. When multiple OMPS/LP profiles corresponded to a single OSIRIS observation, their average was used. To unify the data format, the ozone concentration unit (mol/m $\frac{3}{2}$) of OSIRIS profiles is converted to number density (/cm $\frac{3}{2}$).

Fig. 12 shows the average profiles and relative differences between the retrieval results of this study and OSIRIS v7.3, involving approximately 44,000 profiles. The results indicate that compared with OSIRIS v7.3, the ozone concentration retrieved in this study has a relatively large positive deviation of 28-34% below 18 km; above 35 km, the positive deviation increases with increasing altitude; in the 20-35 km altitude range, except near 23 km, most of the deviations between the two are controlled within 5%.

Fig. 13 further compares the average profiles in the tropics and southern high latitudes, as well as the relative differences of the five latitude zones, with shaded areas indicating the standard deviations. In terms of data sample size,





there are approximately 17,000 profiles in the tropical region, about 10,000 in the northern high latitudes, and around 7,000 in the southern high latitudes. The analysis shows that the northern mid-high latitudes have a significant negative deviation of 5-13% at 21-25 km altitude, which is more prominent in polar regions; the difference in the southern mid-latitudes at 20-36 km altitude is less than 4%, and the consistency in the Antarctic region at 23-35 km altitude is better than 2.5%; most of the deviations in the tropical region at 26-36 km altitude are within 2%. In addition, the differences in the region below 20 km are significant, with the relative difference in the tropical region exceeding 50% and reaching 30% at 13 km in the southern mid-latitude zone.

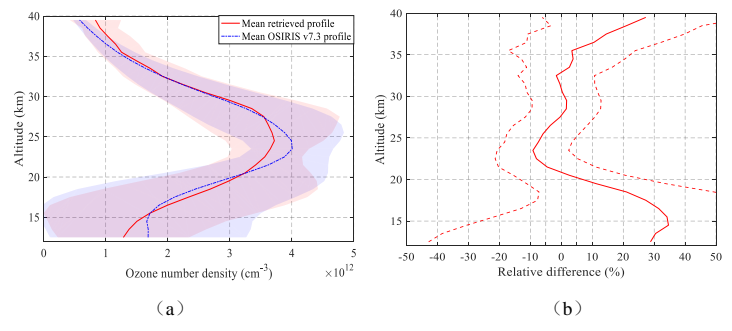


Figure 12. (a) Annual mean ozone number density profiles from this study and OSIRIS v7.3, accompanied by standard deviations (shaded areas); (b) The corresponding annual mean relative differences, accompanied by standard deviations (dashed lines).

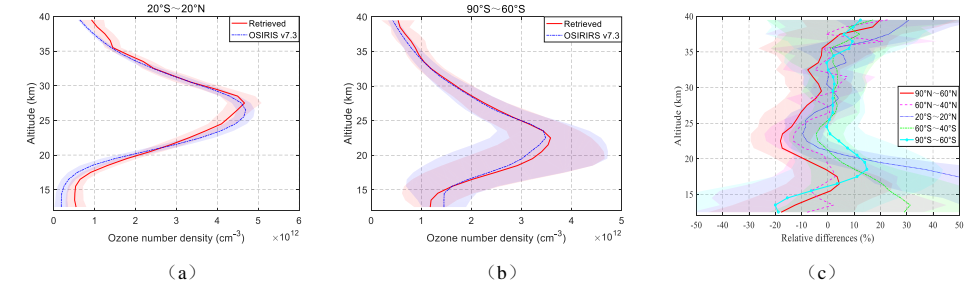


Figure 13. (a, b) Annual mean ozone number density profiles (this study vs. MLS v5.0) for the tropics and Antarctic, respectively. (c) Zonal mean relative differences for five latitudinal bands (60 °-90 N, 40 °-60 N, 20 S-20 N, 60 °-40 S, 90 °-60 S); standard deviations as shaded areas.

4.5 Comparison with ozonesondes

To robustly validate the retrieved ozone concentrations at altitudes below 30 km, this study employs a comparative analysis with ozonesonde measurements. The sonde data were obtained from the World Ozone and Ultraviolet Radiation Data Centre (WOUDC) and the Southern Hemisphere Additional Ozonesondes (SHADOZ) network (Thompson et al., 2007). Accounting for the sparse spatial distribution of ozonesonde stations, a relaxed collocation criterion was implemented: an OMPS/LP measurement was considered a match if it fell within ±5 ° latitude and ±10 ° longitude of a sonde station and occurred within ±12 hours of its launch. For each ozonesonde profile, all collocated OMPS/LP retrievals were averaged to form a single comparative data point.

In quantitative comparisons, to align the vertical resolution of ozonesonde data with that of OMPS data, a moving average filtering method is used for dimensionality reduction of ozonesonde data. The specific procedure begins with defining the window size of the moving average filter:





$$446 N = \frac{\Delta z_{\text{low}}}{\Delta z_{\text{high}}} (8)$$

where, Δz_{low} and Δz_{high} represent the low vertical resolution of OMPS data and the high vertical resolution of ozonesonde data, respectively.

Filtering is applied to the original ozonesonde data x_{fine} to obtain the dimensionality-reduced data x_{coarse} , which is expressed as:

451
$$x_{\text{coarse}}(z_k) = \frac{1}{2N+1} \sum_{j=-N}^{N} x_{\text{fine}}(z_{k+j})$$
 (9)

where z_k denotes the altitude, and k represents the layer index.

In addition, another processing approach involves convolving ozonesonde measurements with the averaging kernels (AKs) retrieved from OMPS/LP v2.6 (see Arosio et al., (2018) for details). Taking the Alert station (82.5 N, 62.4 W) as an example, Fig. 14 presents the comparison results between the ozonesonde data and the collocated OMPS average profile on September 15, 2021. It is found that there are differences in the dimensionality-reduced ozonesonde data obtained by the two methods. The data curve processed by convolution with averaging kernels is smoother and its shape is closer to the OMPS product; while the data processed by moving average filter retains more original features with a sharper curve. After comprehensive consideration, the moving average filter is finally adopted for data processing in this study.

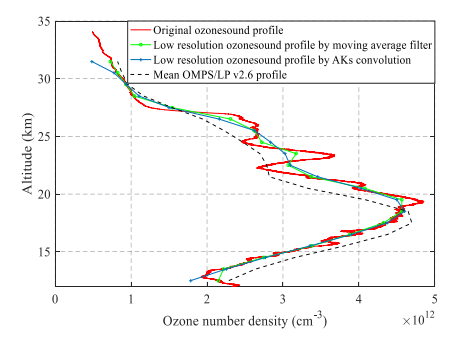
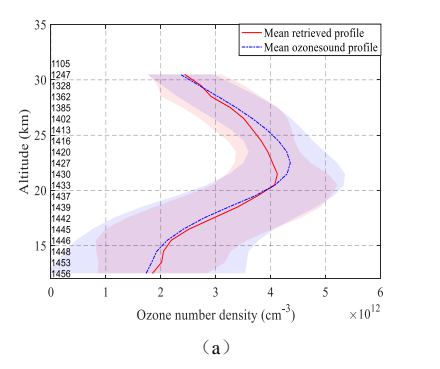


Figure 14. Ozonesonde data and OMPS collocated average profile at Alert station on September 15, 2021

Figure 15 presents the annual average collocated profiles and their relative differences. The left side of the figure denotes the number of valid collocations at each altitude, with the total sample size amounting to approximately 1460. This study included data from 41 ozonesonde stations, involving over 1700 individual profiles. A significant positive bias of 10–15% is observed in the retrievals compared to ozonesonde data below 18 km, while the deviation generally stays within 10% across the 15–30 km altitude range.

Fig. 16 presents the average collocated profiles in the tropical and Antarctic regions, as well as the relative differences across five latitude zones. The left side of the figure indicates that the number of available collocations in the tropical and Antarctic regions is approximately 200 and 75, respectively. Specifically, the tropical region shows good consistency above 20 km, with most relative differences within ±4% between 20 and 30 km. The southern mid-latitude region also exhibits high consistency, with positive biases generally less than 5% above 20 km, but a relatively large positive bias of about 19% near 15 km. In the Antarctic region, the bias is less than 2% above 25 km, while significant differences occur below 25 km, with a positive bias as high as 21% at 19 km. The northern mid-latitude zone has a bias of less than 5% below 21 km, but a constant negative bias of 5-11% between 21-28 km, and this negative bias are more pronounced in the Arctic region.





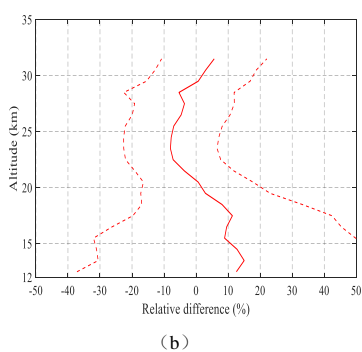
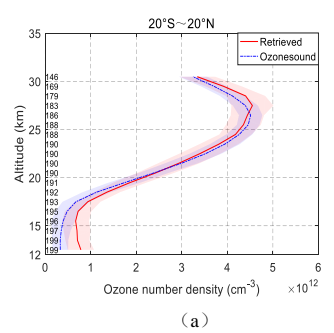
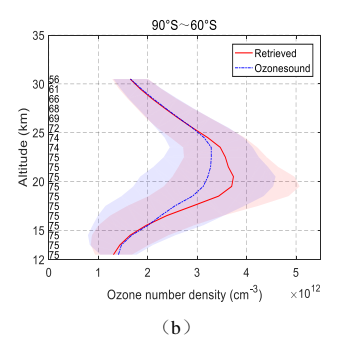


Figure 15. (a) Annual mean collocated ozone number density profiles from this study and ozonesonde measurements, accompanied by standard deviations (shaded areas). (b) The corresponding annual mean relative differences, accompanied by standard deviations (dashed lines).





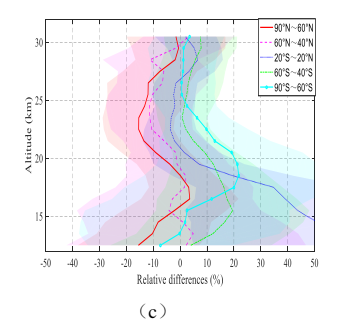


Figure 16. (a, b) Annual mean collocated ozone number density profiles (retrieval vs. ozonesondes) for the tropics and Antarctic, respectively. (c) Zonal mean relative differences for five latitudinal bands ($60^{\circ}-90^{\circ}$ N, $40^{\circ}-60^{\circ}$ N, $20^{\circ}-20^{\circ}$ N, $60^{\circ}-40^{\circ}$ S, $90^{\circ}-60^{\circ}$ S); standard deviations as shaded areas.

5. Conclusions

This study innovatively applies the ozone profile retrieval method—originally developed at the University of Saskatchewan for OSIRIS measurements and based on wavelength pairing and the MART—to OMPS/LP observations. After processing and analyzing the 2021 annual OMPS/LP v2.6 L1G data, observations with the instrument's central slit and solar zenith angle less than 85° were selected, and ozone profiles between 12.5 and 39.5 km were retrieved. A comprehensive multi-dimensional validation was conducted.

Comparison with the NASA L2 v2.6 official product shows that the overall consistency is good across latitude zones at 20-36 km, with most differences within $\pm 5\%$. However, differences near 33 km in the northern mid-latitudes and polar regions reach up to 10%. Below 20 km, ozone concentrations are relatively high in the Antarctic ozone peak region, with a pronounced positive bias around 15 km in tropical and southern mid-latitude zones.

Validation against MLS v5.0 and OSIRIS v7.3 ozone profiles, as well as ozonesonde data from SHADOZ and WOUDC, indicates that relative differences with MLS are mostly within $\pm 10\%$ between 13–35 km, except for significant discrepancies in the tropical UTLS region. Compared to OSIRIS v7.3, a negative bias of 13-18% occurs at 20-25 km in northern mid-high latitudes, while positive biases reach 18% at 18 km over Antarctic and exceed 20% at 15 km in





southern mid-latitudes, with more pronounced deviations in the tropics. Relative to ozonesonde data, differences in tropical and southern mid-latitude regions at 20-30 km remain within ±4%, whereas differences of 11-15% are observed at 20-25 km in northern mid-high latitudes. Consistency is good below 20 km in northern mid-latitudes, but positive biases reach 21% at 18 km over Antarctica and 19% at 15 km in southern mid-latitudes.

Overall, compared with the reference products, the retrieved ozone concentrations in this study exhibit biases mostly within 5% between 25-35 km. A negative bias of 5-10% is observed at 20-25 km in northern mid-high latitudes, particularly in the Arctic. Retrieved values are about 10% higher at the altitude of the Antarctic ozone concentration peak, 10–15% higher at 15 km in southern mid-latitudes, and over 30% higher below 20 km in the tropics.

The identified biases mainly arise from three factors: below 20 km, cloud influence remains non-negligible. Even after excluding cloud-affected radiances, retrieval of lower-altitude ozone profiles is still affected by the initial profile and the adjustment factor above clouds, leading to ozone concentrations more than 25% higher above cloud tops. Inaccurate prior profiles in the mid- to low latitude regions introduce retrieval biases exceeding 20%, while low ozone abundance, strong dynamical variability in the tropics, and reduced sensitivity of limb retrievals further exacerbate discrepancies. Additionally, differences between the background aerosols used in retrievals and real atmospheric conditions also contribute. The elevated concentrations above 35 km across latitude zones result from the limited capability of visible spectra for high-altitude ozone, retrieval, unlike the official product, which uses combined ultraviolet and visible spectra.

Based on error analysis, follow-up research will focus on optimizing the retrieval algorithm, adopting more realistic prior profiles, and constraining the retrieval altitude to cloud-top height. Efforts will also be directed toward deriving aerosol profiles from limb radiance measurements to improve the forward model. This study successfully demonstrates the feasibility of applying the wavelength pairing and MART technique to OMPS/LP ozone profile retrieval, laying a solid technical foundation for broader application of this approach. It also underscores the importance of consistent retrieval settings for constructing long-term, coherent stratospheric ozone datasets and minimizing discrepancies in multi-satellite data merging.

Data availability

Ancillary information and v2.6 L1G OMPS/LP data were downloaded from https://disc.gsfc.nasa.gov/datasets (NASA, 2025a), where L2 data are also available. For the validation sections, MLS L2 data were also taken from https://disc.gsfc.nasa.gov/datasets (Schwartz, et al., 2020). OSIRIS v7.3 data were taken from https://research-groups.usask.ca/osiris/data-products.php (University of Saskatchewan, 2025). WOUDC data were downloaded on 10 April 2025 from https://woudc.org/data/explore.php. A list of all contributors is available on the following website: https://tropo.gsfc.nasa.gov/shadoz/Archive. Html (NASA, 2025b).

Author contributions

FZ designed the retrieval algorithm to OMPS/LP observations, processed the data set, performed the validation of the results and wrote the manuscript. FZ and SWL proposed the research and lead the project, analyzed the results and contributed to the writing of the manuscript and the scientific outcomes. XPL contributed the algorithm for cloud filtering, and reviewed the paper. FQS supervised and guided the retrieval process and reviewed the paper.





538 Competing interests

The authors declare that they have no conflict of interest.

Acknowledgements

- 541 This work was supported by the National Science Foundations of China (Grant No. 41875040), and partially funded
- by the Excellent Research and Innovation Team of Anhui Provincial Department of Education (2023AH010043)
- We would like to express our sincere gratitude to the NASA OMPS SIPS team for providing data support. We are also thanks to the SCIATRAN radiative transfer model development team.

545 References

- 546 Arosio, C., Rozanov, A., Malinina, E., Eichmann, K., von Clarmann, T., and Burrows, J. P.: Retrieval of ozone profiles
- 547 from OMPS limb scattering observations, Atmos. Meas. Tech., 11, 2135-2149,
- 548 https://doi.org/10.5194/amt-11-2135-2018, 2018.
- 549 Arosio, C., Rozanov, A., Gorshelev, V., Laeng, A., and Burrows, J. P.: Assessment of the error budget for stratospheric
- ozone profiles retrieved from OMPS limb scatter measurements, Atmos. Meas. Tech., 15, 5949-5967,
- 551 https://doi.org/10.5194/amt-15-5949-2022, 2022.
- 552 Bernath, P. F., McElroy, C. T., Abrams, M. C., Boone, C. D., Butler, M., Camy-Peyret, C., Carleer, M., Clerbaux, C.,
- Coheur, P. F., Colin, R., DeCola, P., De Mazière, M., Drummond, J. R., Dufour, D., Evans, W. F. J., Fast, H., Fussen,
- D., Gilbert, K., Jennings, D. E., Llewellyn, E. J., Lowe, R. P., Mahieu, E., McConnell, J. C., McHugh, M., McLeod, S.
- D., Michaud, R., Midwinter, C., Nassar, R., Nichitiu, F., Nowlan, C., Rinsland, C. P., Rochon, Y. J., Rowlands, N.,
- 556 Semeniuk, K., Simon, P., Skelton, R., Sloan, J. J., Soucy, M.-A., Strong, K., Tremblay, P., Turnbull, D., Walker, K. A.,
- 557 Walkty, I., Wardle, D. A., Wehrle, V., Zander, R., and Zou, J.: Atmospheric Chemistry Experiment (ACE): Mission
- 558 overview, Geophysical research letters, 32, L15S01, https://doi.org/10.1029/2005GL022386. 2005.
- 559 Bertaux, J. L., Kyrola, E., Fussen, D., Hauchecorne, A., Dalaudier, F., Sofieva, V., Tamminen, J., Vanhellemont, F.,
- Fanton d'Andon, O., Barrot, G., Mangin, A., Blanot, L., Lebrun, J. C., Perot, K., Fehr, T., Saavedra, L., Leppelmeier,
- G. W., and Fraisse, R.,: Global ozone monitoring by occultation of stars: an overview of GOMOS measurements on
- 562 ENVISAT, Atmos. Chem. Phys., 10, 12091–12148, http://doi.org/10.5194/acp-10-12091-2010, 2010.
- 563 Bogumil, K., Orphal, J., and Burrows, J. P.: Temperature dependent absorption cross sections of O₃, NO₂, and other
- atmospheric trace gases measured with the SCIAMACHY spectrometer, in: Proceedings of the
- 565 ERS-Envisat-Symposium, Goteborg, Sweden, 2000.
- Burrows, J., Hölzle, E., Goede, A., Visser, H., and Fricke, W.: SCIAMACHY-Scanning imaging absorption spectrometer
- 567 for atmospheric chartography, Acta Astronautica, 35, 445–451, https://doi.org/10.1016/0094-5765(94)00278-T, 1995.
- 568 Cisewski, M., Zawodny, J., Gasbarre, J., Eckman, R., Topiwala, N., Rodriguez-Alvarez, O., Cheek, D., Hall S.: The
- 569 Stratospheric Aerosol and Gas Experiment (SAGE III) on the International Space Station (ISS) Mission, in:
- Proceedings 9241, Sensors, Systems, and Next-Generation Satellites XVIII, SPIE Remote Sensing, Amsterdam,
- 571 Netherlands, https://doi.org/10.1117/12.2073131, 2014.
- 572 Chen, Z., DeLand, M., and Bhartia, P. K.: A new algorithm for detecting cloud height using OMPS/LP measurements,





- 573 Atmos. Meas. Tech., 9, 1239–1246, https://doi.org/10.5194/amt-9-1239-2016, 2016.
- 574 Chipperfield, M. P. and Bekki, S.: Opinion: Stratospheric ozone-depletion, recovery and new challenges, Atmos. Chem.
- 575 Phys., 24, 2783–2802, https://doi.org/10.5194/acp-24-2783-2024, 2024.
- 576 Degenstein, D. A., Bourassa, A. E., Roth, C. Z., and Llewellyn, E. J.: Limb scatter ozone retrieval from 10 to 60 km
- 577 using a multiplicative algebraic reconstruction technique, Atmos. Chem. Phys., 9, 6521-6529,
- 578 https://doi.org/10.5194/acp-9-6521-2009, 2009.
- 579 DeLand, M., Bhartia, P., Xu, P., Kramarova, N., and Zhu, T.: OMPS Limb Profiler Ozone Product O₃: Version 2.5 Data
- Release Notes, 2017.
- Flittner, D. E., Bhartia, P. K., and Herman, B. M.: O₃ Profiles Retrieved from Limb Scatter Measurements: Theory,
- 582 Geophysical research letters, 27(17), 2601-2604, https://doi.org/10.1029/1999GL011343, 2000.
- 583 Flynn, L., Long, C., Wu, X., Evans, R., Beck, C., Petropavlovskikh, I., McConville, G., Yu, W., Zhang, Z., Niu, J., Beach,
- E., Hao, Y., Pan, C., Sen, B., Novicki, M., Zhou, S., and Seftor, C.: Performance of the ozone mapping and profiler
- suite (OMPS) products, J. Geophys. Res.-Atmos., 119, 6181–6195, https://doi.org/10.1002/2013JD020467, 2014.
- 586 Jia, J., Rozanov, A., Ladst ätter-Wei ßenmayer, A., and Burrows, J. P.: Global validation of SCIAMACHY limb ozone data
- 587 (versions 2.9 and 3.0, IUP Bremen) using ozonesonde measurements, Atmos. Meas. Tech., 8, 3369–3383,
- 588 https://doi.org/10.5194/amt-8-3369-2015, 2015.
- 589 Jaross, G., Bhartia, P. K., Chen, G., Kowitt, M., Haken, M., Chen, Z., Xu, P., Warner, J., Kelly, T.: OMPS Limb Profiler
- instrument performance assessment, J. Geophys. Res.-Atmos., 119, 4399–4412, https://doi.org/10.1002/2013JD020482,
- 591 2014
- Jaross, G.: OMPS-NPP L1G LP Radiance EV Wavelength-Altitude Grid swath orbital 3slit V2.6, Greenbelt, MD, USA,
- 593 Goddard Earth Sciences Data and Information Services Center (GES DISC), Accessed: February 10, 2024,
- 594 https://doi.org/10.5067/YVE3FSNJ59RQ, 2023.
- Kneizys, F. X.: Users Guide to LOWTRAN 7[M]. Air Force Geophysics Laboratory, 1988.
- 596 Kramarova, N. A., Nash, E. R., Newman, P. A., Bhartia, P. K., McPeters, R. D., Rault, D. F., Seftor, C. J., Xu, P. Q., and
- 597 Labow, G. J.: Measuring the Antarctic ozone hole with the new Ozone Mapping and Profiler Suite (OMPS), Atmos.
- 598 Chem. Phys., 14, 2353–2361, https://doi.org/10.5194/acp-14-2353-2014, 2014.
- 599 Kramarova, N. A., Pawan K. Bhartia, Glen Jaross, Leslie Moy, Philippe Xu, Zhong Chen, Matthew DeLand, Lucien
- 600 Froidevaux, Nathaniel Livesey, Douglas Degenstein, Adam Bourassa, Kaley A. Walker, and Patrick Sheese. Validation
- of ozone profile retrievals derived from the OMPS LP version 2.5 algorithm against correlative satellite measurements.
- 602 Atmos. Meas. Tech., 11, 2837–2861, https://doi.org/10.5194/amt-11-2837-2018, 2018.
- 603 Kramarova, N. A., Xu, P., Mok, J., Bhartia, P. K., Jaross, G., Moy, L., Weaver, C., Frith, S., Ziemke, J., Chen, Z., Kahn,
- D., Nyaku, E., Li, J., Davis, S., and Jia, Y.: Ten Year Ozone Profile Record From Suomi NPP OMPS Limb Profiler,
- National Oceanic and Atmospheric Administration Washington D.C., District of Columbia, United States, Technical
- Review NASA Peer Committee December 21, 2022.
- 607 Kramarova, N. A.: OMPS-NPP L2 LP Ozone (O3) Vertical Profile swath daily Center slit V2.6, Greenbelt, MD, USA,
- Goddard Earth Sciences Data and Information Services Center (GES DISC), Accessed: November, 2023,
 10.5067/8MO7DEDYTBH7, 2023.
- Kramarova, N. A., and DeLand, M.: OMPS Limb Profiler Ozone Product O3: Version 2.6 Data Release Notes, 36pp,2023.
- 612 Kramarova, N.A., Xu, P., Mok, J., Bhartia, P. K., Jaross, G., Moy, L., Chen, Z., Frith, S., DeLand, M., Kahn, D., Labow,
- 613 G., Li, J., Nyaku, E., Weaver, C., Ziemke, J., Davis, S., and Jia, Y.: Decade-long Ozone Profile Record from Suomi
- NPP OMPS Limb Profiler: Assessment of Version 2.6 Data, Earth and Space Science, 11, e2024EA003707,
- 615 https://doi.org/10.1029/2024EA003707, 2024.
- 616 Li, F., Newman, P. A., and Waugh, D. W.: Impacts of stratospheric ozone recovery on southern ocean temperature and





- heat budget, Geophysical Research Letters, 50(18), e2023GL103951, https://doi.org/10.1029/2023GL103951, 2023.
- 618 Li, Z., Bi, J., Hu, Z., Ma, J., Li, B.: Regional transportation and influence of atmospheric aerosols triggered by Tonga
- 619 volcanic eruption, Environmental Pollution, 325, 121429, https://doi.org/10.1016/j.envpol.2023.121429, 2023.
- 620 Livesey, N. J., Read, W. G., Wagner, P. A., Froidevaux, L., Santee, M. L., Schwartz, M. J., Lambert, A., Mill án Valle, L.
- 621 F., Pumphrey, H. C., Manney, G. L., Fuller, R. A., Jarnot, R. F., Knosp, B. W., and Lay, R. R.: Version 5.0x Level 2 and
- 3 data quality and description document, available at: https://mls.jpl.nasa.gov/data/v5-0_data_quality_document.pdf
- 623 (last access: June 10, 2025), 2022.
- 624 Llewellyn, E. J., Lloyd, N. D., Degenstein, D. A., Gattinger, R. L., Petelina, S. V., Bourassa, A. E., Wiensz, J. T., Ivanov,
- 625 E. V., McDade, I. C., Solheim, B. H., McConnell, J. C., Haley, C. S., von Savigny, C., Sioris, C. E., McLinden, C. A.,
- 626 Griffioen, E., Kaminski, J., Evans, W. F. J., Puckrin, E., Strong, K., Wehrle, V., Hum, R. H., Kendall, D. J. W.,
- 627 Matsushita, J., Murtagh, D. P., Brohede, S., Stegman, J., Witt, G., Barnes, G., Payne, W. F., Piché, L., Smith, K.,
- Warshaw, G., Deslauniers, D.-L., Marchand, P., Richardson, E. H., King, R. A., Wevers, I., McCreath, W., Kyr d ä, E.,
- Oikarinen, L., Leppelmeier, G. W., Auvinen, H., Mégie, G., Hauchecorne, A., Lefèvre, F., de La Nüe, J., Ricaud, P.,
- Frisk, U., Sjoberg, F., von Schéele, F., and Nordh, L.: The OSIRIS Instrument on the Odin Spacecraft, Canadian
- 1718A, C., Sjoberg, F., von Schere, F., and Politin, E.: The OSIACS Institution of the Outh Spacecraft,
- Journal of Physics, 82(6), 411-422, https://doi.org/10.1139/p04-005, 2004.
- 632 Moy, L., Bhartia, P. K., Jaross, G., Loughman, R., Kramarova, N., Chen, Z., Taha, G., Chen, G., and Xu, P.: Altitude
- registration of limb-scattered radiation, Atmos. Meas. Tech., 10, 167–178, https://doi.org/10.5194/amt-10-167-2017,
- 634 2017.
- 635 NASA: OMPS data, available at: https://disc.gsfc.nasa.gov/datasets, last access: February 2025a.
- NASA: SHADOZ data, available at: https://tropo.gsfc.nasa.gov/shadoz/Archive.html, last access: March 2025b.
- Qian, Y. Y., Luo, Y. H., Zhou, H. J., Yang, T. P., Xi, L., and Si, F. Q.: First Retrieval of Total Ozone Columns from EMI-2
- Using the DOAS Method, Remote Sensing, 16(5): 1234-1245, https://doi.org/10.3390/rs15061665, 2024.
- 639 Rault, D. F. and Loughman, R. P.: The OMPS Limb Profiler Environmental Data Record Algorithm Theoretical Basis
- Document and Expected Performance, Ieee Transactions on Geoscience and Remote Sensing, 51(5): 2505-2527,
- 641 https://doi.org/10.1109/TGRS.2012.2213093, 2013.
- 642 Roth, C. Z., Degenstein, D. A., Bourassa, A. E, and Llewellyn, E. J.: The retrieval of vertical profiles of the ozone
- number density using Chappuis band absorption information and a multiplicative algebraic reconstruction technique,
- Canadian Journal of Physics, 85(11), 1225-1243, https://doi.org/10.1139/p07-130, 2007.
- Rozanov, V. V., Dinter, T., Rozanov, A. V., Wolanin, A., Bracher, A., and Burrows J.P.: Radiative transfer modeling
- through terrestrial atmosphere and ocean accounting for inelastic processes: Software package SCIATRAN. Journal of
- Quantitative Spectroscopy & Radiative Transfer, 194, 65-85, https://doi.org/10.1016/j.jqsrt.2017.03.009, 2017.
- 648 Schwartz, M., Froidevaux, L., Livesey, N., and Read, W.: MLS/Aura Level 2 Ozone (O3) Mixing Ratio V005, Greenbelt,
- MD, USA, Goddard Earth Sciences Data and Information Services Center (GES DISC), Accessed: June 10, 2025,
- 650 https://doi.org/10.5067/Aura/MLS/DATA2516, 2020.
- 651 Thompson, A. M., Witte, J. C., Smit, H. G., Oltmans, S. J., Johnson, B. J., Kirchhoff, V. W., and Schmidlin, F. J.: Southern
- Hemisphere Additional Ozonesondes (SHADOZ) 1998-2004 tropical ozone climatology: 3. Instrumentation,
- station-to-station variability, and evaluation with simulated flight profiles, J. Geophys. Res.-Atmos., 112,
- https://doi.org/10.1029/2005JD007042, 2007.
- University of Saskatchewan: OSIRIS data. available at: https://research-groups.usask.ca/osiris/data-products.php, last
- 656 access: July 25, 2025.
- 657 Veefkind, J. P., de Haan, J. R., Brinksma, E. J., Kroon, M., and Levelt, P. F.: Total ozone from the Ozone Monitoring
- 658 Instrument (OMI) using the DOAS technique, Ieee Transactions on Geoscience and Remote Sensing, 44(5):
- 659 1239-1244, https://doi.org/10.1109/TGRS.2006.871204, 2006.
- Waters, J.W., Froidevaux, L., Harwood, R. S., Jarnot, R. F., Pickett, H. M., and Read, W. G.: The Earth Observing System

https://doi.org/10.5194/egusphere-2025-5580 Preprint. Discussion started: 1 December 2025 © Author(s) 2025. CC BY 4.0 License.





661 Microwave Limb Sounder (EOS MLS) on the Aura satellite, Ieee Transactions on Geoscience and Remote Sensing, 662 44(5), 1075-1092, https://doi.org/10.1109/TGRS.2006.873771, 2006. 663 Xu, P. Q., Bhartia, P. K., Jaross, G. R., DeLand, M. T., Larsen, J. C., Fleig, A., Kahn, D., Zhu, T., Chen, Z., Gorkavyi, N., 664 Warner, J., Linda, M., Chen, H. G., Kowitt, M., Haken, M., and Hall, P.: Release 2 data products from the Ozone Mapping and Profiling Suite (OMPS) Limb Profiler, Proc. SPIE 9242, Remote Sensing of Clouds and the Atmosphere 665 666 XIX, and Optics in Atmospheric Propagation and Adaptive Systems XVII, 92420K (17 October 2014), 667 https://doi.org/10.1117/12.2067320, 2014. 668 Young, P. J., Harper, A. B., Huntingford, C., Paul, N. D., Morgenstern, O., Newman, P. A., Oman, L. D., Madronich, S., 669 and Garcia, R. R.: The Montreal Protocol protects the terrestrial carbon sink, Nature 596, 384-388, https://doi.org/10.1038/s41586-021-03737-3, 2021. 670 671 Zhu, F., Li, S.W., Yang, T. P., and Si, F. Q.: Research on Inversion and Application of Ozone Profile Based on OMPS Limb Scattering Observation, Acta Optica Sinica, 45(6), 82-92, https://doi.org/10.3788/AOS202141.0401005, 2025. 672 673 Zhu, F., Si, F. Q., Zhan, K., Dou, K., and Zhou, H. J.: Inversion of Ozone Profile of Limb Radiation in Chappuis-Wulf 674 Band. Acta Optica Sinica, 41(4), 39-48, https://doi.org/10.3788/AOS241244, 2021. 675 Zhu F., Si, F. Q., Zhou, H. J., Dou, K., Zhao, M. J., and Zhang, Q.: Sensitivity Analysis of Ozone Profiles Retrieved from SCIAMACHY Limb Radiance Based on the Weighted Multiplicative Algebraic Reconstruction Technique, Remote 676 677 Sensing, 14(16), 3954, https://doi.org/10.3390/rs14163954, 2022. 678 679 680 681 682 683 684 685